AMERICAN SOCIETY FOR MICROBIOLOGY | Antimicrobial Agents and Chemotherapy®

SUSCEPTIBILITY

Deletion of *ADA2* Increases Antifungal Drug Susceptibility and Virulence in *Candida glabrata*

Shang-Jie Yu,[a] Ya-Lin Chang,[a] Ying-Lien Chen[a]

[a]Department of Plant Pathology and Microbiology, National Taiwan University, Taipei, Taiwan

ABSTRACT *Candida glabrata*, the second most frequent cause of candidiasis after *Candida albicans*, is an emerging human fungal pathogen that is intrinsically drug tolerant. Currently, studies of *C. glabrata* genes involved in drug tolerance are limited. Ada2, a component serving as a transcription adaptor of the Spt-Ada-Gcn5 acetyltransferase (SAGA) complex, is required for antifungal drug tolerance and virulence in *C. albicans*. However, its roles in *C. glabrata* remain elusive. In this study, we found that *ada2* mutants demonstrated severe growth defects at 40°C but only mild defects at 37°C or 25°C. In addition, *C. glabrata ada2* mutants exhibited pleiotropic phenotypes, including susceptibility to three classes of antifungal drugs (i.e., azoles, echinocandins, and polyenes) and cell wall-perturbing agents but resistance to the endoplasmic reticulum stressor tunicamycin. According to RNA sequence analysis, the expression of 43 genes was downregulated and the expression of 442 genes was upregulated in the *ada2* mutant compared to their expression in the wild type. *C. glabrata ADA2*, along with its downstream target *ERG6*, controls antifungal drug tolerance and cell wall integrity. Surprisingly, *ada2* mutants were hypervirulent in a murine model of systemic infection, possibly due to the upregulation of multiple adhesin-like genes, increased agar invasion, and overstimulation of murine tumor necrosis factor alpha production.

KEYWORDS *Candida glabrata*, antifungal drug susceptibility, cell wall integrity, hypervirulence

The opportunistic human fungal pathogen *Candida glabrata* is the most common non-*albicans Candida* species that causes infections of mucosal surfaces or the bloodstream (i.e., systemic infection) in most geographic regions (1, 2). The rate of mortality from systemic infections caused by *C. glabrata* is relatively high, partly due to its rapidly evolving resistance to antifungal drugs, especially azoles (3, 4). The treatment of *C. glabrata* infections is challenging due to the limited knowledge of *C. glabrata* pathogenicity, the restricted antifungal drug susceptibility of *C. glabrata*, and the availability of few effective antifungal agents.

Infection with *Candida* species is initiated through adherence to host epithelial tissue and colonization within the host (5). In *Candida albicans*, the agglutinin-like sequence (Als) protein family and Hwp1 play crucial roles in adherence to host epithelial cells (6, 7). Similar to the Als family of *C. albicans*, the main adhesins in *C. glabrata* are those of the epithelial adhesin (EPA) family, which facilitate attachment to host epithelial cells and macrophages (8–10). After colonization on host cells, *Candida* cells destroy host tissues and undergo invasive growth, during which proteases, such as the secreted aspartyl proteases (Saps), and phospholipases act as key virulence factors (11–13). Additionally, the unique extracellular glycosylphosphatidylinositol (GPI)-linked aspartyl protease gene family (*YPS* genes) plays important roles in virulence and survival within macrophages (14).

Several studies have reported on the *C. glabrata* genes that are involved in virulence suppression. The most well characterized of these genes is *C. glabrata ACE2* (*CgACE2*), a transcription factor that acts as a negative regulator of virulence in a model of

Received 18 September 2017 **Returned for modification** 6 November 2017 **Accepted** 15 December 2017

Accepted manuscript posted online 8 January 2018

Citation Yu S-J, Chang Y-L, Chen Y-L. 2018. Deletion of *ADA2* increases antifungal drug susceptibility and virulence in *Candida glabrata*. Antimicrob Agents Chemother 62:e01924-17. https://doi.org/10.1128/AAC.01924-17.

Copyright © 2018 American Society for Microbiology. All Rights Reserved.

Address correspondence to Ying-Lien Chen, ychen28@ntu.edu.tw.

systemic infection in immunocompromised mice (15). The evolved (Evo) strain, which has a single nucleotide mutation in the chitin synthase gene *CHS2*, is another hypervirulent *C. glabrata* strain (16). Both the *ace2* mutant and the Evo strain have enhanced virulence; stimulate inflammatory response factors, such as tumor necrosis factor alpha (TNF-α) and interleukin-6 (IL-6); and exhibit a clumpy pseudohypha-like structure. Other strains with enhanced virulence include a strain with the *PDR1* gain-of-function mutation, a strain with mitochondrial dysfunction, and the *anp1* and *mnn2* glycosylation mutants (17–19).

The Spt-Ada-Gcn5 acetyltransferase (SAGA) complex is conserved in eukaryotes and influences the expression of approximately 10% of genes in the *Saccharomyces cerevisiae* genome (20, 21). Within the SAGA complex, Gcn5 is a histone acetyltransferase that mediates nucleosomal acetylation, and the site specificity of lysine acetylation on histones is potentiated by Ada2 and Ada3 (22). In *S. cerevisiae*, the loss of Ada2 results in slow growth under minimal glucose and low-phosphate conditions, temperature sensitivity, and sensitivity to the cell wall-perturbing agent Congo red (CR) (23–25). In *C. albicans*, the *ada2/ada2* mutant is sensitive to Congo red, the endoplasmic reticulum (ER) stressor tunicamycin (TM), and antifungal drugs, such as caspofungin (CSF) and fluconazole (FLC) (26, 27). Meanwhile, the *C. albicans ada2/ada2* mutant exhibits hyphal growth defects and attenuated virulence in murine systemic and *Caenorhabditis elegans* infection models (27, 28). In *Cryptococcus neoformans*, the *ada2* mutant has severe growth defects at 39°C, and *C. neoformans* Ada2 (CnAda2) is required for capsule formation and virulence in a murine intranasal infection model (29). In the filamentous fungus *Aspergillus nidulans*, the *adaB* mutant has defects in growth, conidiation, and conidiophore formation (30). In the rice pathogen *Fusarium fujikuroi*, the *ada2* mutant has impaired growth in solid media (31). However, the roles of *C. glabrata* Ada2 on growth, antifungal tolerance, and virulence have remained elusive.

In this study, we report that *C. glabrata* Ada2 has multiple roles in cellular functions, ranging from growth and cell wall integrity to antifungal drug tolerance and virulence suppression. Importantly, *ERG6* also mediates cell wall integrity and antifungal drug tolerance. We found that *C. glabrata* mutants lacking *ADA2* are hypervirulent in a murine model of systemic infection; this is distinct from findings in *C. albicans* and *C. neoformans*, indicating a divergent role of Ada2 in controlling virulence in human fungal pathogens. We further show evidence to support the suggestion that the hypervirulence of *C. glabrata ada2* (*Cgada2*) mutants may be due to the upregulation of multiple adhesin-like genes, the enhanced invasive growth of *C. glabrata*, and increased murine TNF-α production.

RESULTS

Ada2 mediates acetylation of H3K9 but not H3K14 in *C. glabrata*. To test the Ada2-mediated chromatin modification in *C. glabrata*, we analyzed the acetylation levels at lysine 9 and lysine 14, the main residues acetylated by the SAGA complex in *S. cerevisiae*, on the *C. glabrata* histone H3 protein (H3K9 and H3K14, respectively) (32). We extracted the total protein from the wild type, the *ada2* mutants, and the complemented strain and performed a Western blot analysis with anti-acetylated H3K9 (anti-H3K9ac) or anti-acetylated H3K14 (anti-H3K14ac) antibody. The acetylation level of H3K9 was lower in *ada2* mutants (Fig. 1A) than the wild-type strain; the *P* values for the significance of the difference between the wild-type strain and *ada2* mutants YSJ4 and YSJ39 were <0.0001 and 0.0005, respectively, based on an unpaired *t* test (Fig. 1B). The H3K9 acetylation level of the complemented strain was similar to that of the wild type. The *P* values for the significance of the difference in the acetylation levels between the complemented strain and the wild type and *ada2* mutants YSJ4 and YSJ39 were 0.1811, <0.0001, and 0.0012, respectively. Unlike the acetylation level of H3K14 in *S. cerevisiae*, the acetylation level of H3K14 in the *C. glabrata ada2* mutants was similar to that in the wild-type and complemented strains ($P > 0.05$). These results indicate the convergent and divergent roles of Ada2 in the acetylation of H3K9 and H3K14, respectively, between *C. glabrata* and *S. cerevisiae* or, alternatively, that Ada2 regulates Gcn5 in *C.*

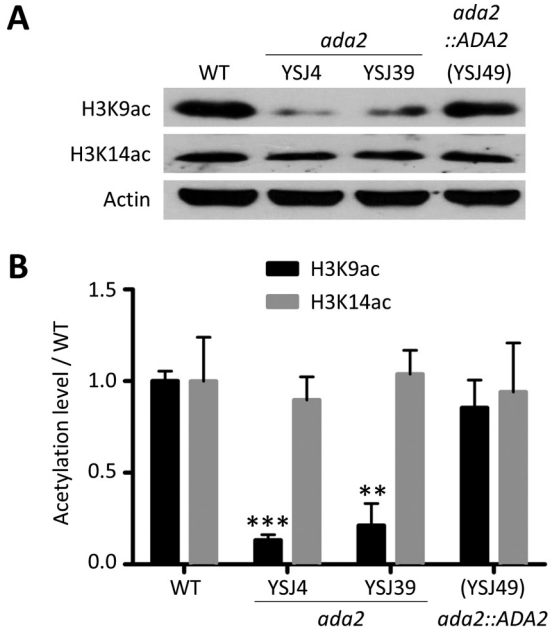

FIG 1 *ADA2* deletion results in decreased acetylation of H3K9 but not H3K14. (A) *C. glabrata* strains were cultured, and the total proteins were extracted to determine the acetylation level of histone 3 via Western blotting. A total of 15 μg of protein was probed with anti-H3K9ac antibody and 45 μg was probed with anti-H3K14ac antibody. Actin was used as a loading control in all blots. (B) Acetylation levels of H3K9 and H3K14 in the *C. glabrata* wild type (WT), the *ada2* mutants, and the complemented strain were determined from three independent Western blot experiments. The blots were analyzed using ImageJ software, and the signals were normalized to the actin signals. The results are represented as the mean ± standard deviation. Asterisks indicate statistically significant differences compared with the results for the wild type using an unpaired *t* test (**, $P < 0.01$; ***, $P < 0.0001$).

glabrata differently than it does in *S. cerevisiae*, based on the finding that H3K14 was acetylated in *S. cerevisiae* but not *C. glabrata*.

Ada2 is required for thermotolerance and growth in *C. glabrata*. *S. cerevisiae ada2* mutants grow slowly in minimal medium and exhibit temperature sensitivity (23), but the role of the *ADA2* gene in *C. glabrata* remains unclear. In spotting assays, *C. glabrata ada2* mutants grew slightly slower on solid YPD than the wild type at 25°C and 37°C but exhibited severe growth defects at 40°C that could be partially rescued with supplementation of the osmotic stabilizer sorbitol (Fig. 2A). We measured the growth kinetics of these strains for 72 h at 25°C, 37°C, and 40°C and found that the *ada2* mutants grew slower at 40°C than at 25°C or 37°C. The complemented strain grew at a rate similar to that of the wild-type strain (Fig. 2B). We measured the growth rate (doubling time) of the wild type, the *ada2* mutants, and the complemented strain in liquid yeast extract-peptone-dextrose (YPD) and found that the *ada2* mutants exhibited a longer doubling time than the wild-type and complemented strains at 25°C and 40°C (Table 1). Interestingly, the *ada2* mutants had a slightly shorter doubling time at 37°C than the wild-type and complemented strains (Table 1).

Ada2 controls antifungal drug tolerance in *C. glabrata*. To determine the role of Ada2 in antifungal drug tolerance, we performed serial dilution spotting, disk diffusion, and MIC assays to determine the role of Ada2 in antifungal drug tolerance. In the serial dilution spotting assay, *ada2* mutants were susceptible to azoles (fluconazole [FLC], posaconazole [PSC], voriconazole [VRC]), echinocandins (micafungin [MCF], caspofungin [CSF], anidulafungin [ANF]), and a polyene (amphotericin B [AmB]) (Fig. 3A). In disk diffusion assays, the *ada2* mutants demonstrated larger and/or clearer inhibition zones in the presence of fluconazole, micafungin, or amphotericin B than the wild-type and complemented strains (Fig. 3B; see also Fig. S2 in the supplemental material). The *ada2* mutants showed 8-fold increased susceptibility to 2 μg/ml fluconazole and 2-fold increased susceptibility to 0.0625 μg/ml micafungin or 0.5

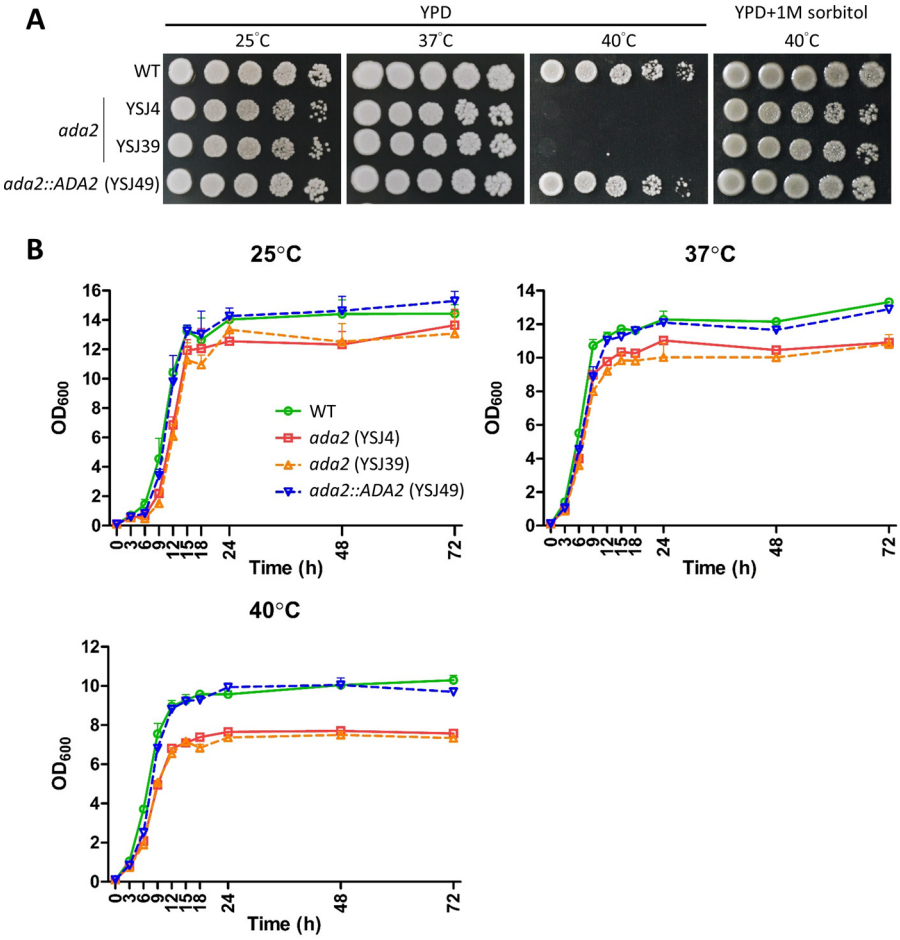

FIG 2 Ada2 is required for thermotolerance and growth. (A) The growth of *ada2* mutants was temperature sensitive, and the osmotic stabilizer sorbitol partially rescued the phenotype at 40°C. Cells were grown overnight in YPD at 37°C and washed twice with dH_2O, 5-fold serially diluted, and spotted onto solid YPD with or without 1 M sorbitol. The cultures were incubated at the indicated temperature for 48 h. (B) Growth kinetics of *C. glabrata* strains at 25°C, 37°C, or 40°C. Cells were grown overnight in liquid YPD at 37°C, washed twice with dH_2O, diluted to an OD_{600} of 0.1 unit/ml in fresh liquid YPD, and incubated at the indicated temperature with shaking at 150 rpm. The OD_{600} of the cultures was measured at 0, 3, 6, 9, 12, 15, 18, 24, 48, and 72 h. The results were plotted using Prism (v5.03) software, and the error bars represent standard deviations from triplicate technical experiments.

μg/ml amphotericin B compared with the susceptibilities of the wild-type and complemented strains (Table 2).

Ada2 is required for cell wall integrity but negatively regulates invasive growth in *C. glabrata*. Most existing antifungal drugs target components or pathways involved in cell wall integrity (33). Since *ada2* mutants are susceptible to three classes

TABLE 1 Doubling time of *C. glabrata* strains at various temperatures

Strain	Doubling time (h) at[a]:		
	25°C	37°C	40°C
Wild type	$2.30 \pm 0.23^{a,b,c}$	$2.04 \pm 0.02^{g,h,i}$	$2.11 \pm 0.08^{m,n,o}$
ada2 mutant (YSJ4)	$2.94 \pm 0.04^{a,d,e}$	$1.86 \pm 0.03^{g,j,k}$	$2.26 \pm 0.07^{m,p,q}$
ada2 mutant (YSJ39)	$4.07 \pm 0.37^{b,d,f}$	$1.89 \pm 0.08^{h,j,l}$	$2.16 \pm 0.02^{n,p,r}$
ada2::*ADA2* mutant (YSJ49)	$2.38 \pm 0.08^{c,e,f}$	$1.95 \pm 0.06^{i,k,l}$	$1.98 \pm 0.01^{o,q,r}$

[a]Data represent the mean $\pm$ standard error of the mean for three technical replicates. In the statistical analyses, *P* values were determined by an unpaired *t* test. The *P* values between two measurements with the same superscript letters were as follows: a, $P = 0.049$; b, $P = 0.015$; c, $P = 0.739$; d, $P = 0.038$; e, $P = 0.003$; f, $P = 0.011$; g, $P = 0.016$; h, $P = 0.191$; i, $P = 0.228$; j, $P = 0.844$; k, $P = 0.345$, l, $P = 0.647$; m, $P = 0.258$; n, $P = 0.614$; o, $P = 0.189$; p, $P = 0.274$; q, $P = 0.021$; r, $P = 0.002$.

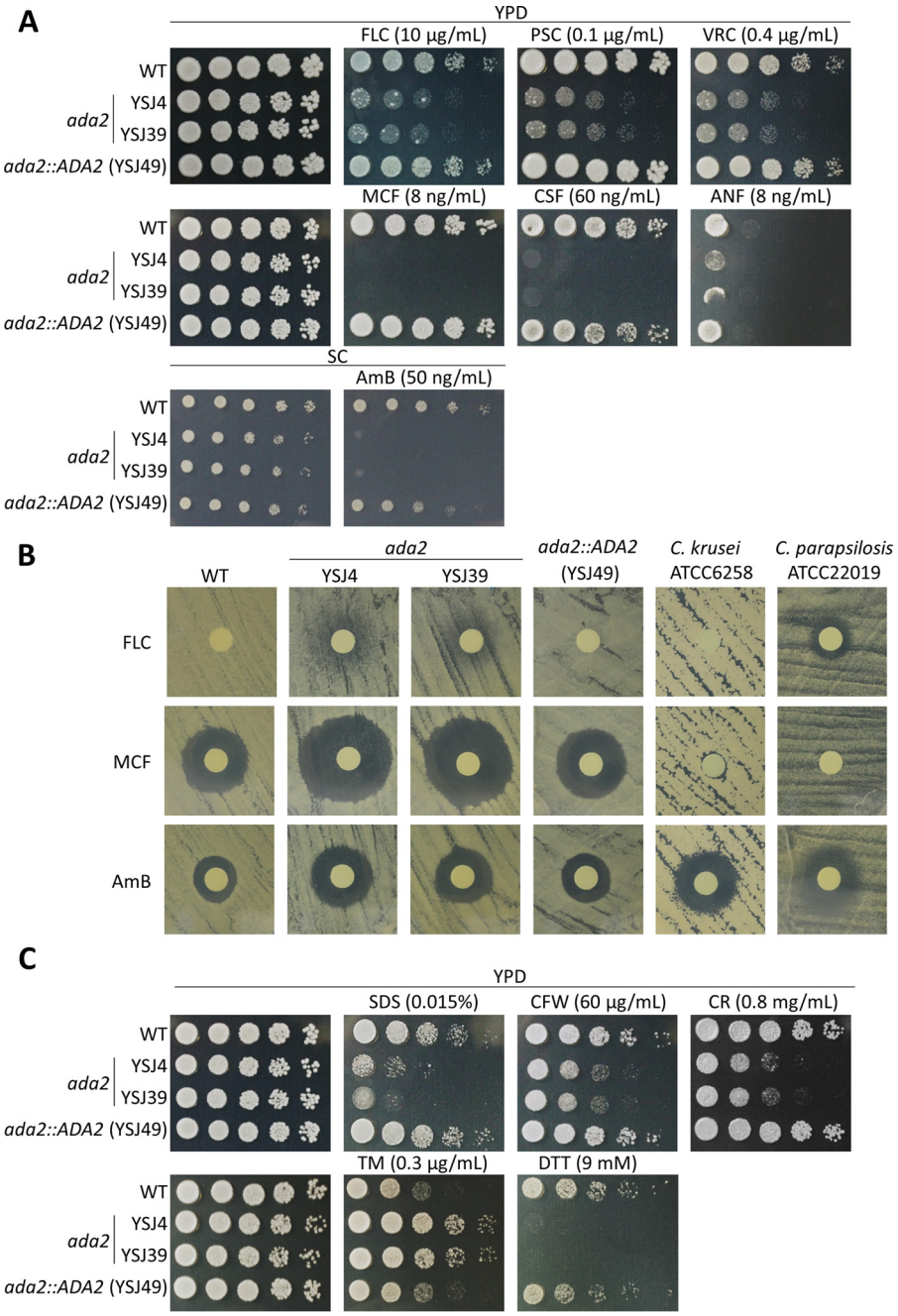

FIG 3 Ada2 controls antifungal drug tolerance and cell wall integrity. (A) The *ada2* mutants were susceptible to azoles, echinocandins, and amphotericin B. Cells were grown overnight in liquid YPD at 37°C, washed twice with dH_2O, 5-fold serially diluted, and spotted onto solid YPD containing fluconazole (FLC), posaconazole (PSC), voriconazole (VRC), micafungin (MCF), caspofungin (CSF), or anidulafungin (ANF) at the indicated concentration. To test susceptibility to amphotericin B (AmB), strains were spotted onto synthetic complete (SC) medium with or without 50 ng/ml AmB. All plates were incubated at 37°C for 30 h. (B) A disk diffusion assay was used to test the susceptibility of the *C. glabrata* strains to FLC, MCF, or AmB. *C. krusei* ATCC 6258 and *C. parapsilosis* ATCC 20019 served as quality control strains. Cells were spread on the surface of Mueller-Hinton agar plus GMB medium plates. Disks containing 20 μg FLC, 40 ng MCF, or 2.5 μg AmB were placed on the agar surface, and the plates were incubated at 35°C for 24 h. (C) The *ada2* mutants are sensitive to cell wall-perturbing agents but resistant to the ER stress chemical tunicamycin. Cells were grown overnight in liquid YPD at 37°C, 5-fold serially diluted, spotted onto solid YPD containing SDS, calcofluor white (CFW), Congo red (CR), dithiothreitol (DTT), or tunicamycin (TM), and incubated at 37°C for 30 h.

TABLE 2 The MICs of *C. glabrata* strains and two quality control *Candida* isolates

Strain	MIC (μg/ml)		
	Fluconazole	Micafungin	Amphotericin B
Wild type	16	0.125	1
ada2 mutant (YSJ4)	2	0.0625	0.5
ada2 mutant (YSJ39)	2	0.0625	0.5
ada2::*ADA2* mutant (YSJ49)	16	0.125	1
C. krusei ATCC 6258	32	0.125	2
C. parapsilosis ATCC 22019	4	2	2

of antifungal drugs, we hypothesized that CgAda2 may play a role in controlling cell wall integrity. To test cell wall integrity in *ada2* mutants, we exposed them to the cell wall-perturbing agents sodium dodecyl sulfate (SDS), calcofluor white (CFW), and Congo red (CR). The *ada2* mutants were sensitive to these agents (Fig. 3C), indicating that Ada2 plays crucial roles in maintaining cell wall integrity. Furthermore, cell separation ability was reduced in *ada2* mutants compared with that in the wild-type and complemented strains (Fig. S1). Because previous studies showed that cell wall integrity is linked with the unfolded protein response (UPR) (34), we investigated whether the UPR was affected in *C. glabrata ada2* mutants when treated with the ER stress inducer tunicamycin (TM; which blocks the synthesis of N-linked glycoproteins in the ER). The tolerance of *ada2* mutants to TM was increased compared with that of the wild-type and complemented strains (Fig. 3C). Interestingly, the *C. glabrata ada2* mutants exhibited enhanced agar invasion compared with the wild-type and complemented strains (Fig. 4A); the *ada2* mutants were observed microscopically to extensively invade agar from both the top and side views compared with the level of invasion by the wild-type and complemented strains (Fig. 4B).

Inactivation of *ADA2* leads to hypervirulence. To study the role of *C. glabrata* Ada2 in virulence, we used a murine model of systemic infection. Immunocompromised mice were infected with a wild-type strain, an *ada2* mutant (YSJ4 or YSJ39), or the complemented strain (YSJ49) in order to determine the survival curve, organ fungal burden, and histopathology. The *ada2* mutants (YSJ4 and YSJ39) showed hypervirulence and produced 100% and 90% mortality, respectively, while the wild-type and complemented strains produced only 40% and 20% mortality, respectively, within 3 weeks postinfection (Fig. 5A). The *P* values for the difference in the rates of mortality between mice infected with the wild-type strain and those infected with *ada2* mutant YSJ4 or YSJ39 were 0.001 and 0.012, respectively, as determined by the log-rank test (Fig. 5A). To determine the ability of *C. glabrata* mutant strains to infect tissues, we performed fungal burden analyses of the spleen, kidneys, and brain. At 48 h postinfection, organs were removed and halved. The organ halves were homogenized, and the homogenates were serially diluted and plated onto solid YPD containing 100 μg/ml chloramphenicol to determine the number of CFU per gram of organ tissue. The *ada2* mutants showed increased fungal burdens in the spleen (YSJ4, $P < 0.0001$; YSJ39, $P = 0.0011$), kidney (YSJ4, $P = 0.0002$; YSJ39, $P = 0.0002$), and brain (YSJ4, $P = 0.0003$; YSJ39, $P = 0.0007$) (*P* values were determined by the Mann-Whitney test), whereas the burden of the complemented strain in the spleen or brain exhibited no difference from that of the wild type, but the burden of the complemented strain in the kidney was slightly lower than that of the wild type ($P = 0.017$) (Fig. 5B). We performed histopathology analysis using the other halves of the organs, which were sliced and periodic acid-Schiff (PAS) stained to visualize colonization of the spleen, kidney, and brain tissues. The *ada2* mutants exhibited a greater ability than the wild-type or complemented strain to colonize the spleen and kidneys (Fig. 5C). However, we did not observe obvious fungal cells in the brain.

***C. glabrata ada2* mutants overstimulate TNF-α production in mice.** Because the *C. glabrata ada2* mutants showed hypervirulence in a murine model of systemic infection, we determined murine TNF-α and IL-6 levels. Mice were infected with the

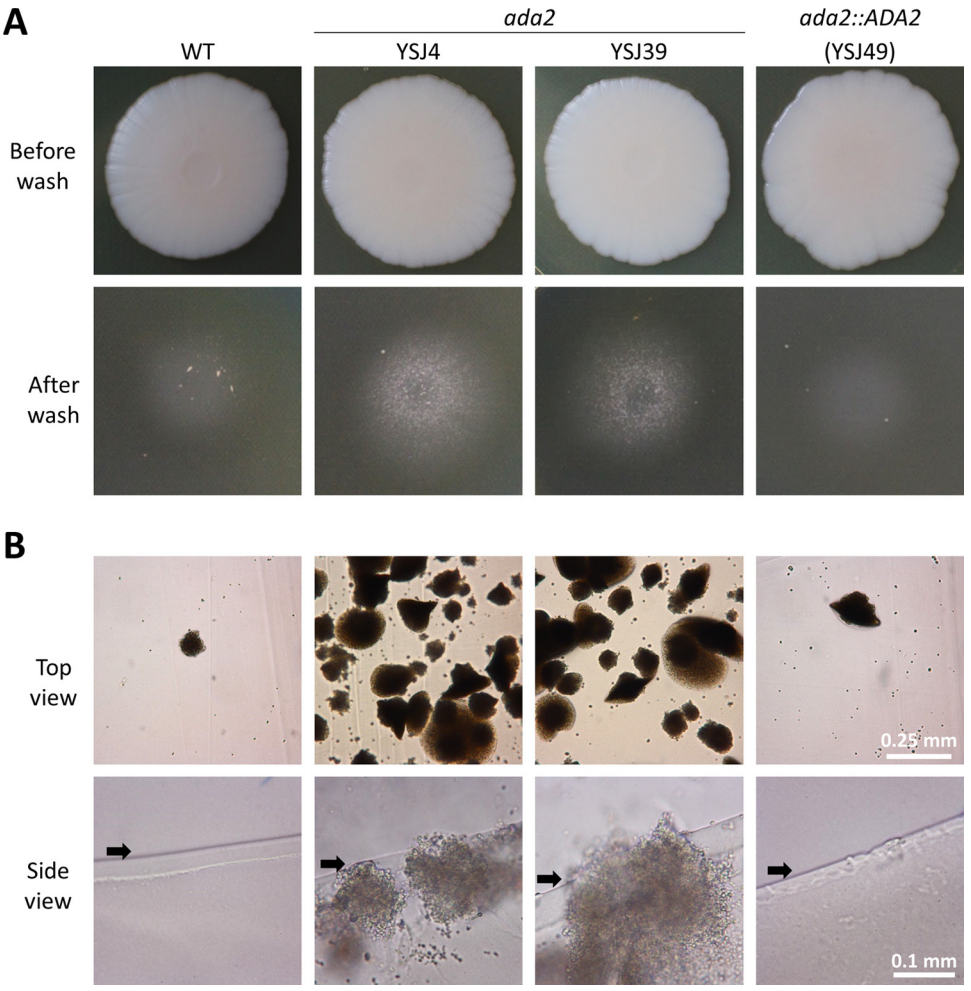

FIG 4 Inactivation of *ADA2* enhances agar invasion. (A) *C. glabrata* strains were grown overnight in YPD at 37°C, washed twice with dH_2O, and diluted to an OD_{600} of 1 unit/ml. Then, 3 μl of cells was spotted onto solid YPD and incubated at 37°C for 10 days. Colonies were photographed before and after washing with dH_2O. (B) The colonies from the assay whose results are shown in panel A were washed, excised, and microscopically observed from the top and side. Arrows, the agar surface.

wild-type strain, an *ada2* mutant, or the complemented strain, and the controls received phosphate-buffered saline (PBS). We collected serum at 18 h postinfection. The levels of TNF-α and IL-6 in PBS-treated mice were undetermined or barely detected, respectively (Table 3). The levels of TNF-α in mice infected with *ada2* mutant YSJ4 or YSJ39 were significantly increased compared with those in mice infected with the wild type ($P = 0.0008$ and $P = 0.0185$, respectively) or the complemented strain ($P < 0.0001$ and $P = 0.0007$, respectively) (P values are based on an unpaired t test). We observed no difference in the levels of IL-6 production between the wild type and the *ada2* mutants (Table 3).

Genome-wide analysis of Ada2-mediated genes in *C. glabrata*. To further understand the pleiotropic phenotypes of *ada2* mutants and identify Ada2-mediated genes in *C. glabrata*, we performed RNA sequencing to compare the genome-wide transcriptome profiles of the wild type and *ada2* mutant YSJ4. Real-time quantitative reverse-transcription PCR (qRT-PCR) analysis confirmed that the transcription of *ADA2* was abolished in the *ada2* mutant (Fig. 6A). A total of 485 genes were differentially regulated (i.e., a >2-fold change in expression was detected) between the *ada2* mutant and the wild-type strain when grown in liquid YPD (Fig. 6B). Among these Ada2-mediated genes, 442 genes were upregulated and 43 were downregulated in the *ada2* mutant. *C. glabrata* contains more adhesin-like genes than other human fungal patho-

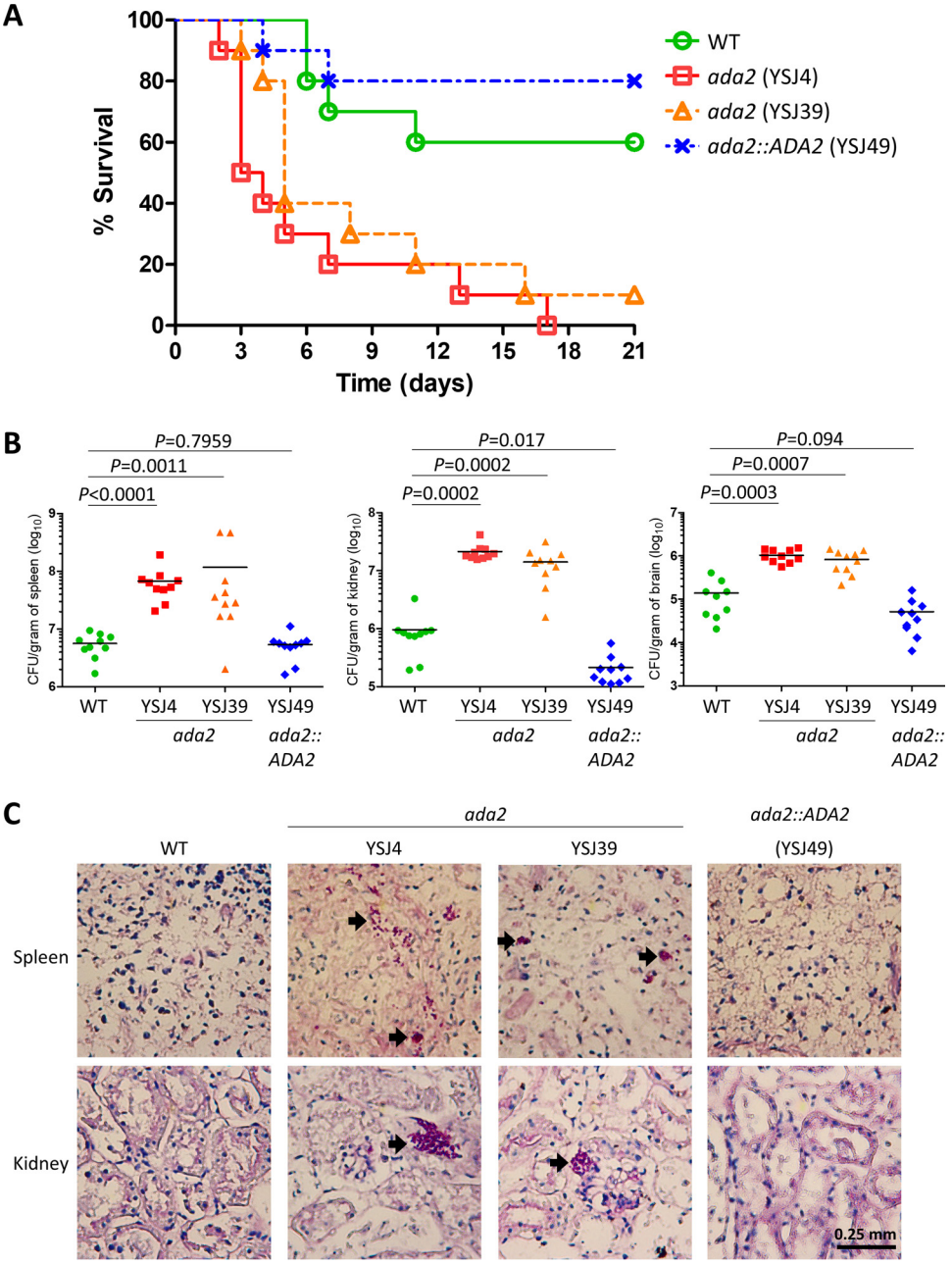

FIG 5 *C. glabrata ada2* mutants are hypervirulent in a model of systemic infection in immunosuppressed mice. (A) Survival curves for mice infected with the wild type, the *ada2* mutants, or the complemented strain. A total of 10 5- to 6-week-old male ICR mice per strain were immunocompromised with cyclophosphamide (200 mg/kg at days −3, 0, and +1). Each mouse was intravenously challenged with 7×10^7 yeast cells in 200 μl of PBS and monitored for 21 days. (B) The fungal burdens of the spleens, kidneys, and brains of the immunocompromised mice were determined at 48 h after challenge with 7×10^7 cells (in 200 μl) via lateral tail vein injection. The *P* values for the significance of the differences between the wild type and the mutants or the complemented strain, based on the log-rank test, are shown. (C) Histopathological sections of spleens and kidneys were dissected from immunocompromised mice infected with 7×10^7 cells of the wild type, the *ada2* mutants, or the complemented strain. The mice were sacrificed at 48 h postinfection. PAS staining was used to observe *C. glabrata* colonization. Arrows, *C. glabrata* cells.

gens; approximately 67 adhesin-like GPI proteins have been found in the *C. glabrata* genome (35). Among the identified upregulated genes, 26 were adhesin-like genes (representing 39% of *C. glabrata* adhesin-like genes); in contrast, only 2 adhesin-like genes (~3% of *C. glabrata* adhesin-like genes) were downregulated (Table 4). Among the 26 upregulated adhesin-like genes were 9 *EPA* genes (*EPA1*, *EPA6*, *EPA8*, *EPA10*,

TABLE 3 TNF-α and IL-6 levels in the blood of mice infected with *C. glabrata* strains

Strain	Cytokine concn[a] (pg/ml)	
	TNF-α	IL-6
Control (PBS)	UD	0.3 ± 0.2
Wild type	39.8 ± 7.5[a,b,c]	411.0 ± 48.1[g,h,i]
ada2 mutant (YSJ4)	130.3 ± 12.9[a,d,e]	410.3 ± 85.8[g,j,k]
ada2 mutant (YSJ39)	101.8 ± 16.9[b,d,f]	336.6 ± 100.6[h,j,l]
ada2::*ADA2* mutant (YSJ49)	10.2 ± 1.6[c,e,f]	216.6 ± 45.5[i,k,l]

[a]Data represent the mean ± standard deviation. In the statistical analyses, *P* values were determined by an unpaired *t* test. The *P* values between two measurements with the same superscript letter were as follows: a, $P = 0.0008$; b, $P = 0.018$; c, $P = 0.0037$; d, $P = 0.218$; e, $P = <0.0001$; f, $P = 0.0007$; g, $P = 0.994$; h, $P = 0.560$; i, $P = 0.022$; j, $P = 0.592$; k, $P = 0.081$; l, $P = 0.308$. UD, undetected.

EPA11, *EPA12*, *EPA15*, *EPA20*, *EPA23*) and 3 *PWP* (PA14 domain-containing wall protein) genes (*PWP2*, *PWP6*, *PWP7*). The two downregulated adhesin-like genes in the *ada2* mutant were *EPA7* and *AWP2*. In addition to the adhesin-like genes, three genes (*YPS4*, *YPS8*, *YPS10*) belonging to the *YPS* gene cluster (14) were also upregulated in the *ada2* mutant. To confirm the reliability of RNA sequencing analysis, we used real-time

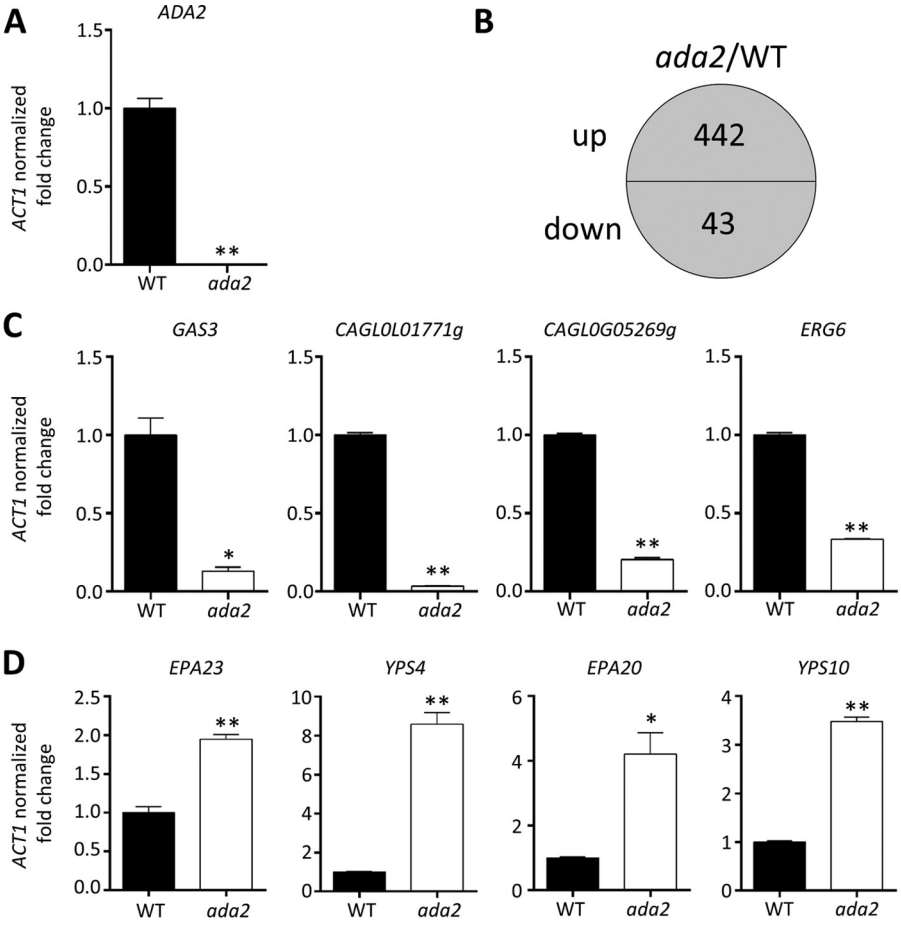

FIG 6 Genes regulated by Ada2 in *C. glabrata*. Strains were grown overnight in liquid YPD at 24°C, washed twice with dH_2O, diluted to an OD_{600} of 0.2 unit/ml with fresh YPD, and incubated at 24°C for 3 h. Log-phase cells were collected for total RNA extraction and further RNA sequencing analyses. (A) The expression of *ADA2*, measured by real-time qRT-PCR, was undetectable in the *ada2* mutant. (B) A total of 485 genes underwent changes in their levels of expression (442 were upregulated and 43 were downregulated) in the *ada2* mutant compared to their levels of expression in the wild type. (C) Real-time qRT-PCR was used to confirm the expression of four downregulated genes (*GAS3* [*CAGL0G1056g*], *CAGL0L01771g*, *CAGL0G05269g*, and *ERG6* [*CAGL0H04653g*]). (D) Real-time qRT-PCR confirmed the expression of *EPA23*, *YPS4*, *EPA20*, and *YPS10*, which were upregulated in the *ada2* mutant. The results are presented as the mean ± standard deviation. Asterisks indicate statistically significant differences compared with the results for the wild type using an unpaired *t* test (*, $P < 0.01$; **, $P < 0.001$).

TABLE 4 Genes regulated by Ada2 in *C. glabrata*

Gene regulation, function, and ORF	Gene	Fold change in expression[a]	*S. cerevisiae* ortholog
Upregulated adhesin/adhesin-like genes (selected, 26/442)			
CAGL0F09273g		8.8	
CAGL0I11011g		8.3	
CAGL0G10219g	*AWP12*	5.2	
CAGL0L00157g		5.1	
CAGL0I10098g	*PWP7*	3.2	*FLO5*
CAGL0I00220g	*EPA23*	2.7	*FLO1*
CAGL0I00110g		2.6	
CAGL0E00110g		2.3	
CAGL0E00275g	*EPA20*	2.2	*FLO5*
CAGL0J00110g		1.8	
CAGL0E01661g		1.8	
CAGL0A01284g	*EPA10*	1.7	*FLO1*
CAGL0C00847g	*EPA8*	1.6	*FLO10*
CAGL0J01774g		1.6	
CAGL0L00227g		1.5	
CAGL0G00110g		1.4	
CAGL0L10092g		1.4	
CAGL0I10246g	*PWP2*	1.3	*FLO1*
CAGL0C00110g	*EPA6*	1.3	*FLO1*
CAGL0E06644g	*EPA1*	1.3	*FLO1*
CAGL0M14069g	*PWP6*	1.2	*FLO9*
CAGL0L13299g	*EPA11*	1.2	*FLO9*
CAGL0M00132g	*EPA12*	1.2	*FLO1*
CAGL0J11968g	*EPA15*	1.2	*FLO5*
CAGL0C00968g		1.2	
CAGL0I07293g		1.1	
Down-regulated genes (43/43)			
Enzyme/enzyme regulator activity			
CAGL0G01056g	*GAS3*	−5.9	*GAS2*
CAGL0A03102g	*ARO10*	−2.4	*ARO10*
CAGL0M00176g	*BAT2*	−1.7	*BAT2*
CAGL0K04235g		−1.5	*NQM1*
CAGL0H04653g	*ERG6*	−1.3	*ERG6*
CAGL0I01166g	*TRR1*	−1.3	*TRR2*
CAGL0J11242g		−1.3	*RHO5*
CAGL0F00363g	*OPI3*	−1.2	*OPI3*
CAGL0F02563g	*HPT1*	−1.2	*HPT1*
CAGL0B01122g	*SAM1*	−1.1	*SAM1*
CAGL0M08602g		−1.1	*CCC2*
CAGL0B00990g	*HBN1*	−1.1	*FRM2*
CAGL0H04081g	*ERG13*	−1.1	*HCS1*
CAGL0K06259g	*TSA1*	−1.1	*TSA2*
Transcription factor/DNA, RNA, protein, or lipid binding activity			
CAGL0L01771g		−4.6	*PHD1*
CAGL0B04213g		−1.6	*RGC1*
CAGL0H08712g		−1.6	
CAGL0H08195g		−1.3	*STI1*
CAGL0B00792g		−1.3	*SRO9*
CAGL0K08756g	*AP5*	−1.2	*YAP5*
CAGL0H05511g		−1.2	*RPS9A*
CAGL0B04675g		−1.2	*DOM34*
CAGL0D05368g		−1.1	*SRB6*
CAGL0K04741g	*SSB2*	−1.0	*SSB2*
Molecular function			
CAGL0G05269g		−2.5	*FMP16*
CAGL0G03531g		−2.2	*SPR6*
CAGL0H07469g		−1.9	*ICS2*
CAGL0G06798g		−1.7	*LSO1*
CAGL0F00187g	*FET4*	−1.2	*FET4*
CAGL0A01474g		−1.2	*SCW11*
CAGL0M00902g		−1.2	*DIF1*

(Continued on next page)

TABLE 4 (Continued)

Gene regulation, function, and ORF	Gene	Fold change in expression[a]	*S. cerevisiae* ortholog
CAGL0L04510g		−1.1	*RPS28A*
CAGL0J11462g		−1.1	*YNL190W*
Transporter			
CAGL0M06281g		−2.4	*DTR1*
CAGL0A02321g	*HXT3*	−1.4	*HXT5*
CAGL0H08393g		−1.2	*BAP2*
CAGL0H10076g		−1.1	*YRO2*
Adhesin/adhesin-like genes			
CAGL0K00110g	*AWP2*	−1.5	
CAGL0C05643g	*EPA7*	−1.1	*FLO9*
Unknown function			
CAGL0F00715g		−1.5	*MAK16*
CAGL0K03069g		−1.3	*IRC21*
CAGL0G06050g		−1.1	

[a]Log_2 ratio, *ada2* mutant/wild type.

qRT-PCR to determine the transcription levels of four upregulated genes (*EPA23*, *EPA20*, *YPS4*, *YPS10*) and four downregulated genes (*GAS3*, *CAGL0L01771g*, *CAGL0G05269g*, *ERG6*). The real-time qRT-PCR results were consistent with the RNA sequencing results (Fig. 6C and D).

***C. glabrata ADA2* mediates antifungal drug tolerance and cell wall integrity via the downstream target *ERG6*.** To identify potential downstream targets of *ADA2*, we disrupted several genes that we found were regulated by *ADA2*, including *GAS3*, *CAGL0L01771g*, and *ERG6*. The *gas3* and *CAGL0L01771g* mutants did not exhibit phenotypes similar to those of the *ada2* mutants (data not shown). Deletion of *ERG6*, a C_{24} sterol methyltransferase involved in the ergosterol biosynthesis pathway, demonstrated echinocandin susceptibility similar to that of the *ada2* mutants, while fluconazole susceptibility was intermediate between that of the wild type and the *ada2* mutants (Fig. 7). In addition, the *erg6* mutants phenocopied *ada2* mutants in terms of sensitivity to the cell wall-perturbing agents SDS, CFW, CR, and dithiothreitol (DTT) (Fig. 7). However, while the *ada2* mutants were tolerant to tunicamycin, the *erg6* mutants showed sensitivity to tunicamycin compared with the wild type (Fig. 7).

DISCUSSION

Roles of Ada2 in thermotolerance and cell wall integrity. Thermotolerance and adaptation to elevated temperatures are important traits for human fungal pathogens to successfully establish infection. The transcription adaptor Ada2 is involved in thermotolerance in several fungi. For example, the *S. cerevisiae ada2* mutant exhibits temperature sensitivity at 37°C (36), while *C. neoformans* strains without *ADA2* have growth defects at 37°C and 39°C (29). In contrast, *C. albicans* Ada2 does not mediate thermotolerance (27). In this study, we showed that *C. glabrata ada2* mutants exhibit severe growth defects at 40°C that can be partially rescued with supplementation of the osmotic stabilizer sorbitol, suggesting that CgAda2 contributes to thermotolerance via maintenance of cell wall integrity. Recent research showed that *S. cerevisiae* SAGA complex subunits, such as Gcn5, are recruited to the promoters of the cell wall integrity response genes in an Slt2-, Rlm1-, and SWI/SNF-dependent manner, and deletion mutants of *GCN5* are sensitive to CR, thus establishing a potential link between the SAGA complex and cell wall integrity (37). However, whether this phenomenon is conserved in *C. glabrata* requires further study.

In this study, we showed that *C. glabrata ada2* mutants are sensitive to elevated temperatures but resistant to the ER stress chemical tunicamycin. Accumulation of unfolded proteins in the ER triggers the unfolded protein response (UPR) pathway, and the ER stress response is related to thermotolerance. For example, in *C. glabrata* the UPR pathway is mainly mediated by the calcineurin pathway and is partially mediated by the Slt2 pathway (38). Inactivation of calcineurin or *SLT2* in *C. glabrata* results in

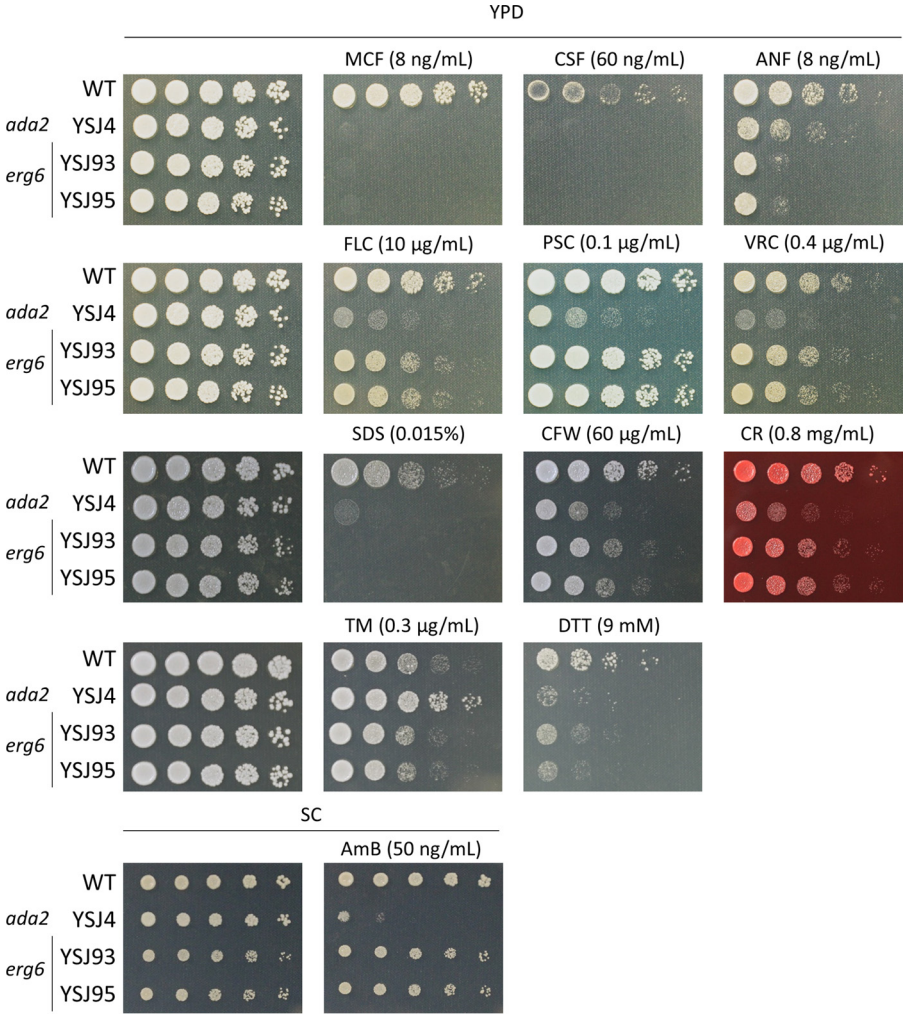

FIG 7 *ADA2* control of antifungal drug tolerance and cell wall integrity is mediated by *ERG6*. The *erg6* mutants were susceptible to echinocandins, fluconazole, cell wall-perturbing agents, and the ER stress chemical tunicamycin but not amphotericin B. Cells were grown overnight in YPD at 37°C and washed twice with dH_2O, 5-fold serially diluted, and spotted onto YPD medium containing MCF, CSF, ANF, FLC, PSC, VRC, SDS, CFW, CR, DTT, or TM at the indicated concentration. Strains were spotted onto SC medium with or without 50 ng/ml AmB to test tolerance to amphotericin B. All plates were incubated at 37°C for 30 h.

increased sensitivity to tunicamycin and elevated temperatures (38–40). Unlike the tunicamycin sensitivity of cell wall-defective strains, such as calcineurin mutants (40), the *C. glabrata ada2* mutants showed resistance to tunicamycin, indicating that *C. glabrata* Ada2 and calcineurin might control tunicamycin tolerance in distinct pathways.

Antifungal drug tolerance. Ada2 controls not only cell wall integrity but also antifungal drug tolerance in *C. glabrata* as well as *C. albicans* (41). It is known that *C. albicans* Ada2 binds to the promoter of the multidrug transporter *CDR1* or the multidrug efflux pump *MDR1*, and the gene expression levels of *CDR1* and *MDR1* in the *C. albicans ada2/ada2* mutant are lower than those in the wild type when exposed to fluconazole (27). However, in *C. glabrata* we did not find that Ada2 regulates ABC transporter-encoding genes, such as *CDR1*, *CDR2* (*PDH1*), or *SNQ2*, based on RNA sequencing results. Possible explanations for this difference may involve divergent roles of Ada2 between *C. glabrata* and *C. albicans* in controlling the expression of the multidrug transporter or efflux pump genes or simply different incubation conditions. In contrast to the *C. glabrata* and *C. albicans* Ada2 proteins, *C. neoformans* Ada2 does not influence fluconazole tolerance (29), suggesting divergent roles of Ada2 in flucona-

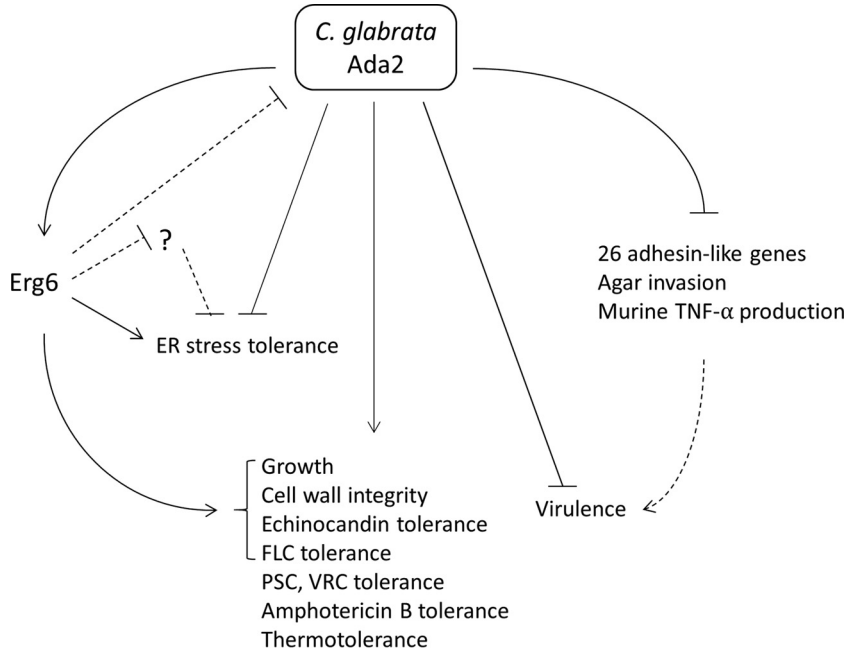

FIG 8 Proposed role of Ada2 in *C. glabrata*. *C. glabrata* Ada2 functions as a positive or a negative regulator governing pleiotropic phenotypes. CgAda2 positively regulates growth, cell wall integrity, and echinocandin and fluconazole (FLC) tolerance, which is mediated at least in part by Erg6. Additionally, Ada2 contributes to tolerance to posaconazole (PSC), voriconazole (VRC), amphotericin B, and thermal stress. Meanwhile, Ada2 negatively regulates, possibly with mediation by Erg6, ER stress tolerance, which potentially inhibits genes such as *ADA2* or other undiscovered genes that negatively regulate ER stress tolerance. Interestingly, Ada2 also negatively regulates virulence in a murine model of systemic infection. The hypervirulence of *ada2* mutants might be caused by the upregulation of multiple adhesin-like genes, increased agar invasion, and overstimulation of murine TNF-α production. Dashed lines, potential relationships.

zole tolerance between *Candida* and *Cryptococcus* species. Meanwhile, this study showed that *Cgada2* mutants are susceptible to amphotericin B, which is distinct from the findings for the *C. neoformans ada2* mutant, which does not exhibit amphotericin B susceptibility (29). However, it is unknown whether the *C. albicans ada2/ada2* mutant is susceptible to amphotericin B.

Hypervirulence. Despite the defects of the *C. glabrata ada2* mutants in cell wall integrity and growth at elevated temperatures (except for a shorter doubling time in liquid medium at 37°C), we found, surprisingly, that the *ada2* mutants have enhanced virulence in a model of systemic infection in immunosuppressed mice. Previous studies showed that *C. albicans ada2/ada2* and *C. neoformans ada2* mutants exhibit attenuated virulence in murine models (27, 29), which is distinct from the increased virulence of the *C. glabrata ada2* mutant, indicating divergent roles of Ada2 in governing virulence between *C. glabrata* and *C. albicans* or *C. neoformans*. The slightly shorter doubling time of the *C. glabrata ada2* mutants in the exponential phase at 37°C might partially explain the observed hypervirulence.

The proinflammatory cytokines TNF-α and IL-6 are crucial for host defense, and their levels reflect the severity of *Candida* infection in humans (42). The *ace2* mutant is the first reported hypervirulent strain in *C. glabrata*, with hypervirulence being attributed to overstimulation of the host cytokines IL-6 and TNF-α (15). For example, the Evo isolate is a hypervirulent *C. glabrata* strain, and infection with this strain results in increased production of IL-6 and TNF-α in the host brain tissue instead of the serum during early murine infection (16). Based on our results, we suggest that the hypervirulence of the *Cgada2* mutants is due at least in part to the overstimulation of TNF-α during murine infection (Table 3 and Fig. 8).

The enhanced agar invasion observed in the *Cgada2* mutants may be linked to the hypervirulent phenotype, although the relationship between agar invasion and viru-

TABLE 5 *Candida* strains used in this study

Species	Strain	Genotype	Parent strain	Reference or source
C. glabrata	CBS138/ATCC 2001	Prototrophic wild type	Clinical isolate	47
C. glabrata	YSJ4	*ada2*Δ::*SAT1*	CBS138	This study
C. glabrata	YSJ39	*ada2*Δ::*SAT1-FLP*	CBS138	This study
C. glabrata	YSJ43	*ada2*Δ::*FRT*	YSJ39	This study
C. glabrata	YSJ49	*ada2*Δ::*FRT*::*ADA2-SAT1*	YSJ43	This study
C. glabrata	YSJ93	*erg6*Δ::*SAT1-FLP*	CBS138	This study
C. glabrata	YSJ95	*erg6*Δ::*SAT1-FLP*	CBS138	This study
C. krusei	CBS573/ATCC 6258	Prototrophic wild type	Clinical isolate	52
C. parapsilosis	CBS604/ATCC 20019	Prototrophic wild type	Clinical isolate	52

lence in *C. glabrata* is unclear. However, *C. glabrata* mutants, such as the *tpo1_1* and *tpo1_2* mutants, which have a reduced agar invasion ability compared with that of the wild type, show reduced virulence in a *Galleria mellonella* infection model (43). Further, the *C. albicans* fluconazole-resistant strain $CO23_{RFLC}$ and the micafungin-resistant strain $CO23_{RFK}$, both of which are derived from the fluconazole- and micafungin-susceptible strain $CO23_S$, showed increased virulence in a murine model of systemic infection and formed branching hyphae that invaded the surface of the agar, unlike the hyphae formed by $CO23_S$, and that were longer than the hyphae formed by $CO23_S$ (44), suggesting a possible relationship between increased virulence and agar invasion in both *C. glabrata* and *C. albicans*. Thus, it is possible that the enhanced agar invasion of *Cgada2* mutants might be linked with hypervirulence (Fig. 4 and 8).

Among a total of 67 *C. glabrata* adhesion genes, 26 genes were upregulated in the *Cgada2* mutant, while only 2 genes were downregulated in the *Cgada2* mutant. Thus, the loss of *ADA2*, resulting in the activation of 26 adhesin-like genes, might potentially contribute to the hypervirulence of *Cgada2* mutants (Table 4 and Fig. 8). Previous research showed that silencing mutations in *C. glabrata* cells can result in the derepression of three *EPA* genes (*EPA1*, *EPA6*, and *EPA7*) and hyperadhesion to several epithelial cell lines (45). For instance, a hyperadherent *C. glabrata sir3* mutant exhibited increased colonization in murine kidneys compared to the wild type (46), suggesting that adherence might be correlated with virulence in *C. glabrata*.

In this study, we demonstrated that *C. glabrata* Ada2 is required for growth, thermotolerance, cell wall integrity, and tolerance to three classes of antifungal drugs. Importantly, Ada2 control of cell wall integrity and antifungal drug tolerance is partially mediated by Erg6. The loss of Ada2 in *C. glabrata* results in hypervirulence in a murine model of systemic infection, which is in contrast to the attenuated virulence seen in *C. albicans* and *C. neoformans ada2* mutants, suggesting a divergent role of Ada2 in governing virulence between different human fungal pathogens. The upregulation of 26 adhesin-like genes, increased agar invasion, and increased TNF-α production in host mice may contribute to the observed hypervirulence (Fig. 8). Future investigations on the signaling pathways and proteins or DNA regions that physically interact with *C. glabrata* Ada2 or other SAGA complex components, such as Ada3 or Gcn5, will allow us to further decipher the mechanisms governing antifungal drug tolerance and virulence in *C. glabrata*.

MATERIALS AND METHODS

Yeast strains, media, and chemicals. The *C. glabrata* strains used in this study are listed in Table 5. Yeast extract-peptone-dextrose (YPD; 1% yeast extract, 2% peptone, 2% glucose) liquid and agar (2%), synthetic complete (SC) medium [0.17% yeast nitrogen base without amino acids, 0.5% $(NH_4)_2SO_4$, 2% glucose, and 2% agar], Mueller-Hinton agar plus GMB medium (Mueller-Hinton agar, 2% glucose, 0.5 μg/ml methylene blue), and RPMI 1640 medium (Sigma, St. Louis, MO, USA) were used in this study. YPD containing 100 μg/ml nourseothricin (Werner BioAgents, Jena, Germany) was used to select transformants. Sodium dodecyl sulfate (SDS; Bioman, New Taipei City, Taiwan), calcofluor white (CFW; Fluorescent Brighter 28; Sigma), Congo red (CR; Genzyme, Cambridge, MA, USA), fluconazole (FLC; Selleckchem, Houston, TX, USA), posaconazole (PSC; Merck, Rahway, NJ, USA), voriconazole (VRC; Sigma), micafungin (MCF; Astellas Pharma Inc., Deerfield, IL, USA), caspofungin (CSF; Merck), anidulafungin (ANF; Pfizer Inc.,

Groton, CT, USA), dithiothreitol (DTT; BioShop, Burlington, ON, Canada), and tunicamycin (TM, Sigma) were added to the media at the concentrations indicated above and below.

Gene disruption and complementation in *C. glabrata*. All deletion mutants were generated from the prototrophic wild-type strain CBS138 (47) using the *SAT1* marker or *SAT1* flipper (48). To disrupt the *ADA2* (*CAGL0K06193g*) gene, approximately 1 kb of the 5′ and 3′ noncoding region (NCR) of the *ADA2* open reading frame (ORF) (for homologous recombination) was PCR amplified with primers JC641/JC764 (for the 5′ NCR) and JC765/JC644 (for the 3′ NCR) (see Table S1 in the supplemental material) from the genomic DNA of the CBS138 strain. The 1.8 kb of the *SAT1* marker was amplified from the plasmid pSFS2A (48) with primers JC723/JC724. Three PCR products, including the 5′ NCR of *ADA2* (5′ *ADA2*^{NCR}), the 5′ NCR of the *SAT1* marker, and the 3′ NCR of *ADA2* (3′ *ADA2*^{NCR}), were treated with the ExoSAP-IT reagent (USB Corp., Cleveland, OH, USA) to remove the remaining primers and deoxynucleoside triphosphates (dNTPs), and we measured the DNA concentration using a SpectraMax 190 microplate reader (Molecular Devices, CA, USA). The products were combined at a 1:3:1 molar ratio (5′ *ADA2*^{NCR}/*SAT1* marker/3′ *ADA2*^{NCR}) to generate an ~3.8-kb disruption cassette by overlap PCR with primers JC641/JC644. Wild-type strain CBS138 was then transformed with 1 to 5 μg of the 5′ *ADA2*^{NCR}-*SAT1* marker-3′ *ADA2*^{NCR} disruption cassette using a modified lithium acetate transformation method (49), and the first nourseothricin-resistant *ada2* mutant (YSJ4) was obtained. To make a second independent nourseothricin-resistant *ada2* mutant, approximately 1 kb of the 5′ and 3′ NCRs of the *ADA2* gene were PCR amplified from the genomic DNA of the CBS138 strain with primers JC885/JC886 (for the 5′ NCR) and JC887/JC888 (for the 3′ NCR). The 3′ and 5′ NCR PCR products of the *ADA2* gene were each digested with two restriction enzymes: SacII/SacI and KpnI/ApaI, respectively. The SacII/SacI-digested PCR products of 3′ *ADA2*^{NCR} were gel purified and cloned into the plasmid pSFS2A, resulting in plasmid pYSJ32 (Table S2). The KpnI/ApaI-digested 5′ *ADA2*^{NCR} PCR products were gel purified and cloned into pYSJ32 to make the *ADA2* disruption plasmid pYSJ36. The pYSJ36 plasmids were digested with KpnI and SacI to release the 5′ *ADA2*^{NCR}–*SAT1-FLP*–3′ *ADA2*^{NCR} disruption cassette and transform the CBS138 strain to obtain YSJ39, the second independent *ada2* mutant with *SAT1-FLP*.

To obtain an *ADA2* complementation strain, we restored the *ADA2* gene in the *ada2* mutant background (YSJ43). *SAT1-FLP* was removed by culturing YSJ39 in YPD medium and replica plating onto nourseothricin-containing medium to confirm the loss of *SAT1-FLP*. Approximately 200 bp of the 5′ NCR and the *ADA2* ORF was PCR amplified from the CBS138 strain with primers JC893/JC894 and digested with the restriction enzymes KpnI and HindIII. The digested PCR products were gel purified and cloned into pYSJ32 to generate the reconstitution plasmid pYSJ46 and then digested with KpnI and SacI to release the complementation cassette 5′ *ADA2*^{NCR}-*ADA2* ORF-*SAT1*-3′ *ADA2*^{NCR}. We transformed this cassette into an *ada2* mutant background (YSJ43) to obtain the *ADA2*-complemented strain YSJ49 (Table 5).

To create an *erg6* mutant, approximately 1 kb of the 5′ and 3′ NCRs of the *ERG6* (*CAGL0H04653g*) gene was PCR amplified from the genomic DNA of the CBS138 strain with primers JC974/JC975 (for the 3′ NCR) and JC972/JC973 (for the 5′ NCR). The 3′ and 5′ NCR PCR products of the *ERG6* gene were each digested with two restriction enzymes: SacII/SacI and KpnI/ApaI, respectively. The SacII/SacI-digested PCR products of 3′ *ERG6*^{NCR} were gel purified and cloned into the plasmid pSFS2A, resulting in the plasmid pYSJ89 (Table S2). We then gel purified the KpnI/ApaI-digested 5′ *ERG6*^{NCR} PCR products and cloned them into pYSJ89 to make the *ERG6* disruption plasmid pYSJ91. The pYSJ91 plasmid was digested with KpnI and SacI to release the 5′ *ERG6*^{NCR}–*SAT1-FLP*–3′ *ERG6*^{NCR} disruption cassette and transform it into the CBS138 strain. YSJ93 and YSJ95, two independent *erg6* mutants derived from two separate transformations, were obtained. All strains were confirmed by amplification of the ORF and 5′ and 3′ NCR integrations of the disruption cassettes.

Determination of acetylation level of H3K9 and H3K14. For Western blot analyses (50), cells were grown overnight at 37°C, diluted to an optical density at 600 nm (OD_{600}) of 0.5 unit/ml with 50 ml fresh YPD broth, and incubated for 4 h at 37°C with shaking at 200 rpm. Cells were then centrifuged, washed once with distilled H_2O (dH_2O), and resuspended in 800 μl extraction buffer (25 mM Tris-HCl, pH 7.4, 0.5 mM EDTA, 0.5 mM EGTA, 10 mM β-mercaptoethanol, 1 μg/ml leupeptin, 1 μg/ml aprotinin, 1 mM phenylmethylsulfonyl fluoride, 1:50 protease inhibitor cocktail [Roche Diagnostics, Mannheim, Germany]). Total protein was isolated using the glass bead method with 0.5-mm-diameter glass beads; samples were homogenized five times for 1 min each time at 1,750 rpm with a 2010 Geno/Grinder homogenizer (Spex SamplePrep, Metuchen, NJ, USA). Samples were placed on ice between each homogenization. Protein concentrations were determined by the Bradford method (Bio-Rad, Hercules, CA, USA). Then, 15 μg (for H3K9ac) or 45 μg (for H3K14ac) of total protein was separated on SDS-PAGE gels and transferred to nitrocellulose membranes. The membranes were blocked with 5% Silk milk (Fonterra, Auckland City, New Zealand) in Tris-buffered saline with Tween 20 (TBST; 20 mM Tris, pH 7.5, 150 mM NaCl, 0.1% Tween 20) and incubated with primary antiactin antibody (catalog number MAB1501; Merck Millipore), anti-H3K9ac antibody (catalog number ab4441; Abcam, Cambridge, MA, USA), or anti-H3K14ac antibody (catalog number ab52946; Abcam, Cambridge, MA, USA) overnight at 4°C with shaking. The membranes were washed five times with TBST buffer and then incubated with secondary horseradish peroxidase-conjugated goat anti-mouse IgG antibody (catalog number AP124P; Merck Millipore, Billerica, MA, USA) or goat anti-rabbit IgG antibody (catalog number ab205718; Abcam, Cambridge, MA, USA). Chemiluminescence signals were detected using an enhanced chemiluminescence system (T-Pro Biotechnology, New Taipei City, Taiwan). The Western blot analyses were repeated three times independently, and signals were analyzed using ImageJ software (https://imagej.nih.gov). The statistical analysis of *P* values was performed using an unpaired *t* test. Bar graphs of the quantity normalized to that of the wild type were created with Prism (v5.03) software.

Serial dilution spotting assays. Cells were grown overnight at 37°C and washed twice with dH_2O. We measured the absorbance of the cells at 600 nm (OD_{600}) with an Ultrospec 10 cell density meter (Amersham Biosciences, Uppsala, Sweden). Cells were resuspended to an OD_{600} of 1 unit/ml with dH_2O, and 3 μl of a 5-fold serial dilution of each strain was spotted onto solid agar plates and incubated at the temperatures and for the times indicated above.

Growth kinetics and doubling time measurement. For growth kinetics assays, cells were grown overnight at 37°C, washed twice with dH_2O, and diluted to an OD_{600} of 0.1 with fresh YPD broth. Then, 5 ml of diluted cells was cultured at 25°C, 37°C, and 40°C with shaking at 150 rpm. We measured the cell concentrations after 0, 3, 6, 9, 12, 15, 18, 24, 48, and 72 h using a SpectraMax 190 microplate reader. The experiments were performed in triplicate, and the data were plotted using Prism (v5.03) software. Measurement of the doubling time of each strain was calculated with the following formula: $T\ln 2/[\ln(OD^T/OD^{T0})]$, where OD^T and OD^{T0} represent the OD_{600} at time T and time zero, respectively (51). The exponential-phase time points from 3 to 9 h were chosen to calculate the doubling time. The *P* values were determined using a nonparametric *t* test.

Observation of cell separation ability. *C. glabrata* strains were grown overnight in YPD broth at 37°C, washed twice with dH_2O, stained with 1 mg/ml calcofluor white (Fluorescent Brighter 28; Sigma) for 5 min at room temperature, and then washed once with dH_2O. Stained cell suspensions were spotted onto slides and visualized at a ×1,000 magnification under a bright field and UV light.

Disk diffusion susceptibility assays. Disk diffusion susceptibility assays with fluconazole, micafungin, and amphotericin B were performed following Clinical and Laboratory Standards Institute (CLSI) guideline M44-A2 (52). In brief, *C. glabrata* strains were plated onto Mueller-Hinton agar plus GMB medium plates, and sterile disks were applied onto the agar surface. Then, 20 μg of fluconazole, 40 ng of micafungin, or 2.5 μg of amphotericin B was dropped into each disk. The plates were incubated for 24 h at 35°C and photographed.

Determination of MICs. To determine the MICs, we followed CLSI guideline M27-A3 (53). In brief, we added 100 μl of serially diluted drugs (2-fold the final concentration) into 100-μl cell suspensions in a 96-well polystyrene plate. The final cell concentrations were between 0.5×10^3 and 2.5×10^3 CFU/ml. The plates were incubated for 24 h at 35°C without shaking. The quality control strains *Candida krusei* ATCC 6258 and *Candida parapsilosis* ATCC 22019 were used to ensure that the drugs, medium, and procedure were reliable.

Agar invasion assay. *C. glabrata* strains were grown overnight in YPD broth at 37°C and washed twice with dH_2O. The cell suspensions were diluted to an OD_{600} of 1 unit/ml, and 3 μl was spotted onto solid YPD medium and incubated at 37°C for 10 days. Cells were removed from the surface by rubbing with gloved fingers, and then the plates were washed with 200 ml dH_2O. Colonies were photographed before and after removal from the agar surface. The agar was excised after the cells were removed from the agar surface. We microscopically observed and photographed the invading cells from the top and side.

Murine model of systemic infection. Animal studies were conducted in the Department of Plant Pathology and Microbiology at National Taiwan University (NTU). The murine systemic infection models were reviewed and approved by the NTU Institutional Animal Care and Use Committee (IACUC) under approval number NTU-102-EL-36.

Five- to 6-week-old male ICR mice (BioLasco Taiwan Co., Ltd.) were used in the study. For the survival test, groups of 10 mice were immunosuppressed with cyclophosphamide (200 mg/kg of body weight; Sigma) at day −3, day 0, and day +1. *C. glabrata* strains were grown in liquid YPD overnight at 37°C with shaking at 200 rpm, washed twice with phosphate-buffered saline (PBS), and resuspended in PBS. The cells were vigorously vortexed for 2 min in order to reduce the clumping of *ada2* mutant cells and then counted with a hemocytometer and diluted with an appropriate amount of PBS to obtain an infection inoculum concentration of 3.5×10^8 cells/ml. Then, 200 μl (7×10^7 cells) was used to infect mice through the lateral tail vein. To assess cell viability, appropriate dilutions of the cells were plated on solid YPD and incubated at 37°C for 48 h. The course of infection was monitored for 21 days. Statistical analyses by the Mantel-Cox log-rank test were used to determine the *P* values for the significance of the difference between the survival curves of each strain; statistical significance was set at a *P* value of <0.05. For fungal burden analyses, 10 mice were immunosuppressed and infected with *C. glabrata* strains as described above. The mice were sacrificed and dissected at 48 h after inoculation. The spleens, kidneys, and brains of *C. glabrata*-infected mice were removed, weighed, and transferred to 2-ml sample tubes containing 1 ml ice-cold PBS. Samples were homogenized with steel beads for 2 min at 1,750 rpm. Tissue homogenates were serially diluted, and 100 μl of each dilution was plated on solid YPD containing 100 μg/ml chloramphenicol and incubated at 37°C for 48 h in order to determine the number of CFU per gram of organ tissue. The identity of the colonies recovered from the organs was confirmed by colony PCR. The *P* values for the significance of the difference between the fungal burdens of each strain were determined via the Mann-Whitney test. For histopathological analyses, half of the spleen and kidney was fixed with 10% formamide (Sigma). Periodic acid-Schiff (PAS) staining was performed at the Department of Veterinary Medicine at National Taiwan University.

Analyses of immune modulators in mice. Five- to 6-week-old male ICR mice (BioLasco Taiwan Co., Ltd.) were used in the study. Mice were immunosuppressed with cyclophosphamide (200 mg/kg; Sigma) at day −3 and day 0. The preparation of the *C. glabrata* inoculum was as described above. Four mice were infected with 7×10^7 cells of the *C. glabrata* wild type (200 μl) by lateral tail vein injection, while five mice were infected with PBS as controls; one mouse from the group infected with the wild type expired during the lateral tail vein injection. Blood was collected via the submandibular blood collection method at 18 h postinfection. The tube of blood was allowed to stand for 1 h and then was centrifuged

for 20 min at 1,750 rpm at room temperature to collect serum, which was stored at −20°C. The interleukin-6 (IL-6) and tumor necrosis factor alpha (TNF-α) serum levels were determined by the use of mouse IL-6 and TNF-α enzyme-linked immunosorbent assay Ready-Set-Go kits (eBioscience, San Diego, CA, USA), respectively. Statistical analysis to determine *P* values for the significance of differences between the groups was performed with an unpaired *t* test.

RNA sequencing experiments. Strains were grown overnight in liquid YPD at 24°C, washed twice with dH_2O, diluted to an OD_{600} of 0.2 unit/ml with fresh YPD, and incubated for 3 h at 24°C with shaking at 250 rpm. Then, 20 ml of the culture was immediately added to 30 ml of methanol precooled to −80°C in order to stop cellular processes and RNase activity. Cells were then centrifuged at −4°C for 10 min at 3,250 rpm. Total RNA was extracted using a RiboPure-Yeast kit (Ambion) and treated with DNase I (Ambion) to degrade contaminating DNA. mRNA was enriched with oligo(dT) magnetic beads. Fragmentation buffer allowed the mRNA to be shortened into ~200-base fragments. Then, the first strand of cDNA was synthesized by the use of a random hexamer, buffer, dNTPs, and RNase H, and the second strand of cDNA was synthesized by the use of DNA polymerase I. The double-stranded cDNAs were purified with magnetic beads. End preparation and 3′ end single nucleotide adenine addition were performed, and sequencing adaptors were ligated to the fragments, which were enriched by PCR amplification. During the quality control step, an Agilent 2100 bioanalyzer and ABI StepOnePlus real-time PCR system were used to qualify and quantify the sample library. The library products were sequenced via an Illumina HiSeq 2000 instrument.

Real-time qRT-PCR. For real-time qRT-PCR, total RNA extracted as described above was treated with the reagents from a Turbo DNA-free kit (Invitrogen, Carlsbad, CA, USA) to eliminate genomic DNA contamination. Then, 2 μg of DNA-free total RNAs was reverse transcribed to cDNA by a high-capacity cDNA reverse transcription kit (Applied Biosystems). The 20-μl reaction volume of the real-time PCR mixtures included 6 μl cDNA (6 ng), 10 μl of 2× quantitative PCR master mix (Fast SYBR green master mix; Applied Biosystems), 2 μl of 2.5 μM forward primer, and 2 μl of 2.5 μM reverse primer. The primers were designed using Primer Express (v3.0) software (Applied Biosystems) (Table S1). Quantitative PCR conditions were as follows: 95°C for 10 min for denaturation, 95°C for 3 s and 60°C for 30 s (40 cycles), 95°C for 15 s, 60°C for 60 s, and 95°C for 15 s (melting curve). A StepOnePlus system and a StepOne (v2.2) system (Applied Biosystems) were used to determine the cycle threshold (C_T) values, and the relative expression levels were calculated on the basis of the $2^{-\Delta\Delta CT}$ value. Bar graphs of the *ACT1*-normalized relative quantity compared with that for the wild type (strain CBS138) were created with Prism (v5.03) software. *P* values for the significance of the difference in the RT-quantitative PCR results between the wild type and the *ada2* mutant (YSJ4) were determined by an unpaired *t* test.

Accession number(s). We deposited the RNA sequences in the NCBI Gene Expression Omnibus (GEO) database under accession number GSE76338 (https://www.ncbi.nlm.nih.gov/geo/query/acc.cgi?acc=GSM1981429).

SUPPLEMENTAL MATERIAL

Supplemental material for this article may be found at https://doi.org/10.1128/AAC.01924-17.

SUPPLEMENTAL FILE 1, PDF file, 0.6 MB.

ACKNOWLEDGMENTS

We thank Joachim Morschhäuser for providing the pSFS2A plasmid and Cecelia Wall for language editing.

This work was financially supported by grants 102-2320-B-002-041-MY2, 104-2320-B-002-063-MY3, and 106-2923-B-002-001-MY3 from the Ministry of Science & Technology and grant 104AS-10.7.3-BQ-B1(5) from the Bureau of Animal and Plant Health Inspection and Quarantine in Taiwan.

REFERENCES

1. Azie N, Neofytos D, Pfaller M, Meier-Kriesche H-U, Quan S-P, Horn D. 2012. The PATH (Prospective Antifungal Therapy) Alliance® registry and invasive fungal infections: update 2012. Diagn Microbiol Infect Dis 73:293–300. https://doi.org/10.1016/j.diagmicrobio.2012.06.012.
2. Guinea J. 2014. Global trends in the distribution of *Candida* species causing candidemia. Clin Microbiol Infect 20:5–10. https://doi.org/10.1111/1469-0691.12539.
3. Pfaller M, Diekema D. 2007. Epidemiology of invasive candidiasis: a persistent public health problem. Clin Microbiol Rev 20:133–163. https://doi.org/10.1128/CMR.00029-06.
4. Klevay MJ, Horn DL, Neofytos D, Pfaller MA, Diekema DJ. 2009. Initial treatment and outcome of *Candida glabrata* versus *Candida albicans* bloodstream infection. Diagn Microbiol Infect Dis 64:152–157. https://doi.org/10.1016/j.diagmicrobio.2009.03.007.
5. Calderone RA, Fonzi WA. 2001. Virulence factors of *Candida albicans*. Trends Microbiol 9:327–335. https://doi.org/10.1016/S0966-842X(01)02094-7.
6. Hoyer LL, Green CB, Oh S-H, Zhao X. 2008. Discovering the secrets of the *Candida albicans* agglutinin-like sequence (ALS) gene family—a sticky pursuit. Med Mycol 46:1–15. https://doi.org/10.1080/13693780701435317.
7. Nobile CJ, Schneider HA, Nett JE, Sheppard DC, Filler SG, Andes DR, Mitchell AP. 2008. Complementary adhesin function in *C. albicans* biofilm formation. Curr Biol 18:1017–1024. https://doi.org/10.1016/j.cub.2008.06.034.
8. Cormack BP, Ghori N, Falkow S. 1999. An adhesin of the yeast pathogen *Candida glabrata* mediating adherence to human epithelial cells. Science 285:578–582. https://doi.org/10.1126/science.285.5427.578.
9. Kuhn DM, Vyas VK. 2012. The *Candida glabrata* adhesin Epa1p causes adhesion, phagocytosis, and cytokine secretion by innate immune cells.

FEMS Yeast Res 12:398–414. https://doi.org/10.1111/j.1567-1364.2011.00785.x.
10. Brunke S, Hube B. 2013. Two unlike cousins: *Candida albicans* and *C. glabrata* infection strategies. Cell Microbiol 15:701–708. https://doi.org/10.1111/cmi.12091.
11. Hube B, Sanglard D, Odds FC, Hess D, Monod M, Schäfer W, Brown A, Gow N. 1997. Disruption of each of the secreted aspartyl proteinase genes *SAP1*, *SAP2*, and *SAP3* of *Candida albicans* attenuates virulence. Infect Immun 65:3529–3538.
12. De Bernardis F, Arancia S, Morelli L, Hube B, Sanglard D, Schäfer W, Cassone A. 1999. Evidence that members of the secretory aspartyl proteinase gene family, in particular *SAP2*, are virulence factors for *Candida* vaginitis. J Infect Dis 179:201–208. https://doi.org/10.1086/314546.
13. Chen Y-L, de Bernardis F, Yu S-J, Sandini S, Kauffman S, Tams RN, Bethea E, Reynolds TB. 2015. *Candida albicans OPI1* regulates filamentous growth and virulence in vaginal infections, but not inositol biosynthesis. PLoS One 10:e0116974. https://doi.org/10.1371/journal.pone.0116974.
14. Kaur R, Ma B, Cormack BP. 2007. A family of glycosylphosphatidylinositol-linked aspartyl proteases is required for virulence of *Candida glabrata*. Proc Natl Acad Sci U S A 104:7628–7633. https://doi.org/10.1073/pnas.0611195104.
15. Kamran M, Calcagno A-M, Findon H, Bignell E, Jones MD, Warn P, Hopkins P, Denning DW, Butler G, Rogers T. 2004. Inactivation of transcription factor gene *ACE2* in the fungal pathogen *Candida glabrata* results in hypervirulence. Eukaryot Cell 3:546–552. https://doi.org/10.1128/EC.3.2.546-552.2004.
16. Brunke S, Seider K, Fischer D, Jacobsen ID, Kasper L, Jablonowski N, Wartenberg A, Bader O, Enache-Angoulvant A, Schaller M. 2014. One small step for a yeast-microevolution within macrophages renders *Candida glabrata* hypervirulent due to a single point mutation. PLoS Pathog 10:e1004478. https://doi.org/10.1371/journal.ppat.1004478.
17. Ferrari S, Ischer F, Calabrese D, Posteraro B, Sanguinetti M, Fadda G, Rohde B, Bauser C, Bader O, Sanglard D. 2009. Gain of function mutations in *CgPDR1* of *Candida glabrata* not only mediate antifungal resistance but also enhance virulence. PLoS Pathog 5:e1000268. https://doi.org/10.1371/journal.ppat.1000268.
18. Ferrari S, Sanguinetti M, De Bernardis F, Torelli R, Posteraro B, Vandeputte P, Sanglard D. 2011. Loss of mitochondrial functions associated with azole resistance in *Candida glabrata* results in enhanced virulence in mice. Antimicrob Agents Chemother 55:1852–1860. https://doi.org/10.1128/AAC.01271-10.
19. West L, Lowman DW, Mora-Montes HM, Grubb S, Murdoch C, Thornhill MH, Gow NA, Williams D, Haynes K. 2013. Differential virulence of *Candida glabrata* glycosylation mutants. J Biol Chem 288:22006–22018. https://doi.org/10.1074/jbc.M113.478743.
20. Wang L, Mizzen C, Ying C, Candau R, Barlev N, Brownell J, Allis CD, Berger SL. 1997. Histone acetyltransferase activity is conserved between yeast and human *GCN5* and is required for complementation of growth and transcriptional activation. Mol Cell Biol 17:519–527.
21. Lee TI, Causton HC, Holstege FC, Shen W-C, Hannett N, Jennings EG, Winston F, Green MR, Young RA. 2000. Redundant roles for the TFIID and SAGA complexes in global transcription. Nature 405:701–704. https://doi.org/10.1038/35015104.
22. Balasubramanian R, Pray-Grant MG, Selleck W, Grant PA, Tan S. 2002. Role of the Ada2 and Ada3 transcriptional coactivators in histone acetylation. J Biol Chem 277:7989–7995. https://doi.org/10.1074/jbc.M110849200.
23. Berger SL, Piña B, Silverman N, Marcus GA, Agapite J, Regier JL, Triezenberg SJ, Guarente L. 1992. Genetic isolation of *ADA2*: a potential transcriptional adaptor required for function of certain acidic activation domains. Cell 70:251–265. https://doi.org/10.1016/0092-8674(92)90100-Q.
24. Hoke SM, Genereaux J, Liang G, Brandl CJ. 2008. A conserved central region of yeast Ada2 regulates the histone acetyltransferase activity of Gcn5 and interacts with phospholipids. J Mol Biol 384:743–755. https://doi.org/10.1016/j.jmb.2008.09.088.
25. Sinha H, David L, Pascon RC, Clauder-Münster S, Krishnakumar S, Nguyen M, Shi G, Dean J, Davis RW, Oefner PJ. 2008. Sequential elimination of major-effect contributors identifies additional quantitative trait loci conditioning high-temperature growth in yeast. Genetics 180:1661–1670. https://doi.org/10.1534/genetics.108.092932.
26. Bruno VM, Kalachikov S, Subaran R, Nobile CJ, Kyratsous C, Mitchell AP. 2006. Control of the *C. albicans* cell wall damage response by transcriptional regulator Cas5. PLoS Pathog 2:e21. https://doi.org/10.1371/journal.ppat.0020021.
27. Sellam A, Askew C, Epp E, Lavoie H, Whiteway M, Nantel A. 2009. Genome-wide mapping of the coactivator Ada2p yields insight into the functional roles of SAGA/ADA complex in *Candida albicans*. Mol Biol Cell 20:2389–2400. https://doi.org/10.1091/mbc.E08-11-1093.
28. Pukkila-Worley R, Peleg AY, Tampakakis E, Mylonakis E. 2009. *Candida albicans* hyphal formation and virulence assessed using a *Caenorhabditis elegans* infection model. Eukaryot Cell 8:1750–1758. https://doi.org/10.1128/EC.00163-09.
29. Haynes BC, Skowyra ML, Spencer SJ, Gish SR, Williams M, Held EP, Brent MR, Doering TL. 2011. Toward an integrated model of capsule regulation in *Cryptococcus neoformans*. PLoS Pathog 7:e1002411. https://doi.org/10.1371/journal.ppat.1002411.
30. Reyes-Dominguez Y, Narendja F, Berger H, Gallmetzer A, Fernandez-Martin R, Garcia I, Scazzocchio C, Strauss J. 2008. Nucleosome positioning and histone H3 acetylation are independent processes in the *Aspergillus nidulans* prnD-prnB bidirectional promoter. Eukaryot Cell 7:656–663. https://doi.org/10.1128/EC.00184-07.
31. Rösler SM, Kramer K, Finkemeier I, Humpf HU, Tudzynski B. 2016. The SAGA complex in the rice pathogen *Fusarium fujikuroi*: structure and functional characterization. Mol Microbiol 102:951–974. https://doi.org/10.1111/mmi.13528.
32. Church M, Smith KC, Alhussain MM, Pennings S, Fleming AB. 2017. Sas3 and Ada2 (Gcn5)-dependent histone H3 acetylation is required for transcription elongation at the de-repressed *FLO1* gene. Nucleic Acids Res 45:4413–4430. https://doi.org/10.1093/nar/gkx028.
33. Cowen LE, Sanglard D, Howard SJ, Rogers PD, Perlin DS. 2014. Mechanisms of antifungal drug resistance. Cold Spring Harb Perspect Med 5:a019752. https://doi.org/10.1101/cshperspect.a019752.
34. Krishnan K, Askew DS. 2014. Endoplasmic reticulum stress and fungal pathogenesis. Fungal Biol Rev 28:29–35. https://doi.org/10.1016/j.fbr.2014.07.001.
35. De Groot PW, Kraneveld EA, Yin QY, Dekker HL, Groß U, Crielaard W, de Koster CG, Bader O, Klis FM, Weig M. 2008. The cell wall of the human pathogen *Candida glabrata*: differential incorporation of novel adhesin-like wall proteins. Eukaryot Cell 7:1951–1964. https://doi.org/10.1128/EC.00284-08.
36. Pina B, Berger S, Marcus GA, Silverman N, Agapite J, Guarente L. 1993. *ADA3*: a gene, identified by resistance to GAL4-VP16, with properties similar to and different from those of *ADA2*. Mol Cell Biol 13:5981–5989. https://doi.org/10.1128/MCB.13.10.5981.
37. Sanz AB, García R, Rodríguez-Peña JM, Nombela C, Arroyo J. 2016. Cooperation between SAGA and SWI/SNF complexes is required for efficient transcriptional responses regulated by the yeast MAPK Slt2. Nucleic Acids Res 44:7159–7172. https://doi.org/10.1093/nar/gkw324.
38. Miyazaki T, Nakayama H, Nagayoshi Y, Kakeya H, Kohno S. 2013. Dissection of Ire1 functions reveals stress response mechanisms uniquely evolved in *Candida glabrata*. PLoS Pathog 9:e1003160. https://doi.org/10.1371/journal.ppat.1003160.
39. Miyazaki T, Inamine T, Yamauchi S, Nagayoshi Y, Saijo T, Izumikawa K, Seki M, Kakeya H, Yamamoto Y, Yanagihara K. 2010. Role of the Slt2 mitogen-activated protein kinase pathway in cell wall integrity and virulence in *Candida glabrata*. FEMS Yeast Res 10:343–352. https://doi.org/10.1111/j.1567-1364.2010.00611.x.
40. Chen Y-L, Konieczka JH, Springer DJ, Bowen SE, Zhang J, Silao FGS, Bungay AAC, Bigol UG, Nicolas MG, Abraham SN. 2012. Convergent evolution of calcineurin pathway roles in thermotolerance and virulence in *Candida glabrata*. G3 (Bethesda) 2:675–691. https://doi.org/10.1534/g3.112.002279.
41. Ramírez-Zavala B, Mogavero S, Schöller E, Sasse C, Rogers PD, Morschhäuser J. 2014. SAGA/ADA complex subunit Ada2 is required for Cap1- but not Mrr1-mediated upregulation of the *Candida albicans* multidrug efflux pump Mdr1. Antimicrob Agents Chemother 58:5102–5110. https://doi.org/10.1128/AAC.03065-14.
42. Netea MG, Van der Graaf CA, Vonk AG, Verschueren I, Van der Meer JW, Kullberg BJ. 2002. The role of Toll-like receptor (TLR) 2 and TLR4 in the host defense against disseminated candidiasis. J Infect Dis 185:1483–1489. https://doi.org/10.1086/340511.
43. Santos R, Costa C, Mil-Homens D, Romão D, Carvalho CC, Pais P, Mira NP, Fialho AM, Teixeira MC. 2017. The multidrug resistance transporters CgTpo1_1 and CgTpo1_2 play a role in virulence and biofilm formation in the human pathogen *Candida glabrata*. Cell Microbiol 19:12686. https://doi.org/10.1111/cmi.12686.
44. Angiolella L, Stringaro AR, De Bernardis F, Posteraro B, Bonito M, Toccacieli L, Torosantucci A, Colone M, Sanguinetti M, Cassone A. 2008.

Increase of virulence and its phenotypic traits in drug-resistant strains of *Candida albicans*. Antimicrob Agents Chemother 52:927–936. https://doi.org/10.1128/AAC.01223-07.
45. Kaur R, Domergue R, Zupancic ML, Cormack BP. 2005. A yeast by any other name: *Candida glabrata* and its interaction with the host. Curr Opin Microbiol 8:378–384. https://doi.org/10.1016/j.mib.2005.06.012.
46. Castaño I, Pan SJ, Zupancic M, Hennequin C, Dujon B, Cormack BP. 2005. Telomere length control and transcriptional regulation of subtelomeric adhesins in *Candida glabrata*. Mol Microbiol 55:1246–1258.
47. Dujon B, Sherman D, Fischer G, Durrens P, Casaregola S, Lafontaine I, De Montigny J, Marck C, Neuvéglise C, Talla E. 2004. Genome evolution in yeasts. Nature 430:35–44. https://doi.org/10.1038/nature02579.
48. Reuß O, Vik Å, Kolter R, Morschhäuser J. 2004. The *SAT1* flipper, an optimized tool for gene disruption in *Candida albicans*. Gene 341:119–127. https://doi.org/10.1016/j.gene.2004.06.021.
49. Gietz D, St Jean A, Woods RA, Schiestl RH. 1992. Improved method for high efficiency transformation of intact yeast cells. Nucleic Acids Res 20:1425. https://doi.org/10.1093/nar/20.6.1425.
50. Burnette WN. 1981. "Western blotting": electrophoretic transfer of proteins from sodium dodecyl sulfate-polyacrylamide gels to unmodified nitrocellulose and radiographic detection with antibody and radioiodinated protein A. Anal Biochem 112:195–203. https://doi.org/10.1016/0003-2697(81)90281-5.
51. Chen Y-L, Yu S-J, Huang H-Y, Chang Y-L, Lehman VN, Silao FGS, Bigol UG, Bungay AAC, Averette A, Heitman J. 2014. Calcineurin controls hyphal growth, virulence, and drug tolerance of *Candida tropicalis*. Eukaryot Cell 13:844–854. https://doi.org/10.1128/EC.00302-13.
52. Clinical and Laboratory Standards Institute. 2009. Method for antifungal disk diffusion susceptibility testing of yeasts; approved guideline M44-A2, 2nd ed. Clinical and Laboratory Standards Institute, Wayne, PA.
53. Clinical and Laboratory Standards Institute. 2008. Reference methods for broth dilution antifungal susceptibility testing of yeasts: approved standard, 2nd ed. Document M27-A3. Clinical and Laboratory Standards Institute, Wayne, PA.